Narrow-band Circularly Polarized Antenna for Medical Microwave Imaging and Health Monitoring Applications

Bilal Guetaf[1], Abdelhalim Chaabane[1], Abderrezak Khalfallaoui[1], and Hussein Attia[2]

[1]Laboratoire des Télécommunications-LT
Département d'Electronique et Télécommunications, Faculté des Sciences et de la Technologie
Université 8 Mai 1945 Guelma, BP 401, Guelma, 24000, Algeria
guettaf.bilal@univ-guelma.dz, abdelhalim.chaabane@univ-guelma.dz, khalfalloui.abderrezak@univ-guelma.dz

[2]Interdisciplinary Research Center for Communication Systems and Sensing, and Electrical Engineering Department
King Fahd University of Petroleum and Minerals, Dhahran, 31261, Saudi Arabia
hattia@kfupm.edu.sa

Abstract – In this paper, a circularly polarized printed monopole antenna (CPPMA) is proposed for medical microwave imaging and health monitoring applications. The proposed CPPMA is optimized to operate at the Industrial, Scientific and Medical (ISM) band. A prototype of the designed antenna is fabricated and printed on the low-cost FR-4 substrate that has a compact size of 34 × 28 × 1.5 mm^3. The simulated results indicate that the designed CPPMA operates between 2.425 GHz and 2.475 GHz while the measured results range between 2.32 GHz and 2.515 GHz. The designed CPPMA also reveals a circular polarization performance at 2.45 GHz (2.4386 GHz - 2.4633 GHz). The suitability of CPPMA for microwave imaging is confirmed by checking its aptitudes to detect the presence of breast tumors and brain strokes. A great detection capability is achieved for breast tumors and brain strokes of various sizes inserted at different positions with a high sensitivity to changes or anomalies in the dielectric properties of human tissues. In addition, the usefulness of the proposed CPPMA for wearable application is justified experimentally. Excellent agreement is achieved between the simulated results and the measured ones.

Index Terms – Breast tumor and brain stroke detection, circularly polarized printed monopole antenna (CPPMA), industrial scientific and medical (ISM) band, medical microwave imaging and health monitoring, phantom models, wearable antenna.

I. INTRODUCTION

The most commonly used medical imaging modalities for image reconstructions of human anatomy, tissues or organs include X-ray computed tomography, mammography, magnetic-resonance imaging, single photon emission computed tomography-computerized tomography (SPECT-CT) and ultrasound. However, each one of these screening approaches are quite costly, painful and ionized [1].

To overcome the drawback of these methods, microwave imaging has gained the interest of many biomedical researchers because of its attractive features that include low-cost, safety, simplicity, high image resolution of the scanned body tissues, non-ionizing radiations and being non-invasive [2]. It is based on mono-static or multi-static radar-type measurements, and benefits from the marked dielectric contrast between healthy and diseased tissues. The mono-static radar imaging system that uses a single antenna to scan the body with mechanical movement is faster and more efficient. Whereas the multi-static radar imaging system that uses an antenna array is complex, expensive and time consuming [3].

Circularly polarized (CP) antennas enhance the performances of medical microwave imaging radar systems since they reduce indoor multi-path effects and body postures, reduce polarization mismatch losses, penetrate lossy dielectric materials of the human body tissues, and provide a robust detection of the tumors irrespective to the antenna orientation constraints [4]. Several antennas have been reported for biomedical applications such as those presented in [5–17], however, these antennas are linearly polarized and have only one use whether for cancer screening, stroke screening, or health monitoring. Thus, novel high-performance antennas are needed for several biomedical applications.

In this paper, a mono-static CPPMA of size 34 × 28 × 1.5 mm^3 is proposed at Industrial, Scientific and Medical (ISM) band for medical microwave imaging applications and health monitoring wearable applications. The proposed CPPMA is capable of detecting

Submitted On: August 21, 2022
Accepted On: May 3, 2023

https://doi.org/10.13052/2023.ACES.J.380607

breast tumors and brain strokes of various sizes inserted at different positions. This CPPMA may also be utilized for remote health monitoring systems because of its operation in the ISM band and circular polarization properties. This remote health monitoring system can keep track of a patient's medical information while they are at home, making it easier to diagnose and treat them as well as forecast when they will get sick and regulate their condition. Additional contributions presented in this work include: 1) the design and the fabrication of a simple and low-cost antenna for several biomedical applications: breast cancer detection, brain stroke detection and for health monitoring and wearable applications; 2) the introduction and the evaluation of the circular polarization performance for the detection of tumors; 3) the ability to detect very small breast tumors and strokes is validated through the use of phantom models; 4) the usefulness of the fabricated prototype for wearable health applications is justified experimentally; 5) the detection of strokes in the human head through the analysis of E-field, H-field and current density; 6) the evaluation of specific absorption rate (SAR) parameters on the breast, head and arm of the human body phantom.

All the simulations presented in this work are carried out using CST Microwave Studio software.

II. ANTENNA AND BODY PHANTOM MODEL DESIGN

A. Antenna design and evolution analysis

Figure 1 presents the geometry of the designed CPPMA. Its optimized dimensions are given in Table 1. Figure 2 shows the evolution of the CPPMA design during the design process, whereas Fig. 3 describes the corresponding reflection coefficient and the axial ratio (AR) of the different designs.

The two slots and a stub inserted on the ground plane are responsible for generation of the circular polarization (AR = 0.98 dB $<$ 3 dB at 2.45 GHz, AR bandwidth ranges from 2.4386 GHz to 2.4633 GHz). This circular polarization performance can also be observed from the surface current direction as the phase augments in time. Figure 4 shows the current distributions on the surface of the proposed CPPMA at 2.45 GHz for four different phases (0°, 90°, 180° and 270°). It can be seen from the results that the main current direction for 0° is in the -X direction, whereas the main current direction for 90° is in the +Y direction. Besides, the main current direction at 180° and 270° are reverse to those of 0° and 90°, respectively. Accordingly, the main surface current turns in a clockwise trend. It signifies that a left-hand circular polarization (LHCP) is acquired in the direction of propagation with the designed CPPMA.

Figure 5 shows the simulated right-hand circularly polarized (RHCP) and LHCP far-field radiation patterns of the antenna in xz-plane (H-plane) and yz-plane (E-plane) at 2.45 GHz. It confirms that the proposed CPPMA radiates LHCP in the direction of the propagation and RHCP in the reverse direction. The minor inclinations of the radiation patterns in xz-plane (H-plane) are due to asymmetric geometry of the designed CPPMA. Comparable results are obtained in [18–19].

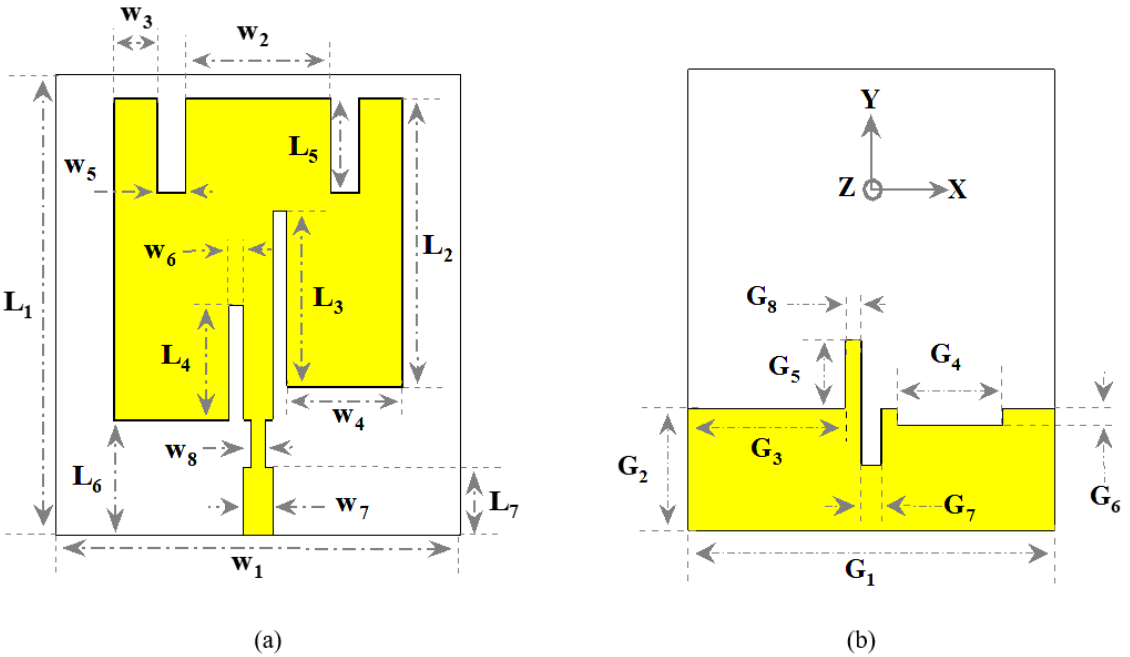

Fig. 1. Geometry of the designed CPPMA: (a) front view, (b) back view.

Table 1: Optimized dimensions of the proposed CPPMA

Parameter	W_1	L_1	W_2	W_3	W_4	W_5	W_6	W_7	W_8	L_2	L_3	L_4
Value (mm)	28	34	3	10	8	2	1	2	1	21.3	13	8.5
Parameter	L_5	L_6	L_7	G_1	G_2	G_3	G_4	G_5	G_6	G_7	G_8	
Value (mm)	7	8.7	5	28	9	12	8	5	1.25	1.6	1.2	

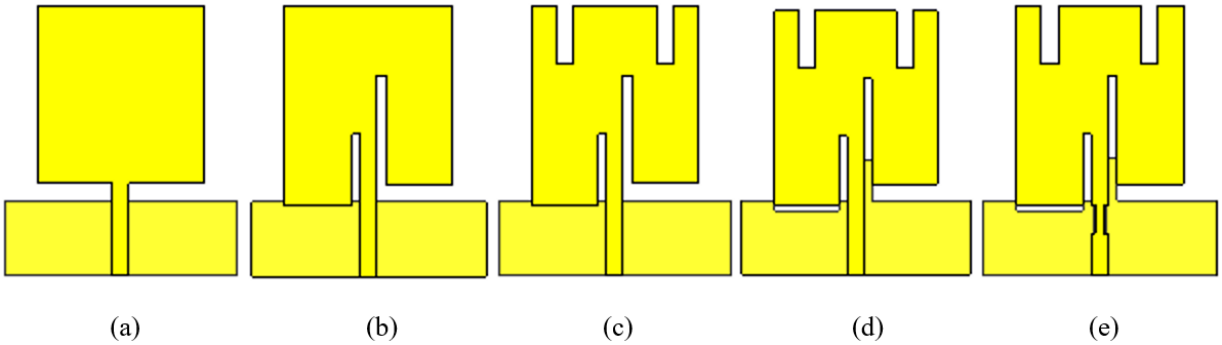

(a) (b) (c) (d) (e)

Fig. 2. The evolution of the proposed CPPMA during the design process: (a) Antenna 1, (b) Antenna 2, (c) Antenna 3, (d) Antenna 4, and (e) Proposed CPPMA.

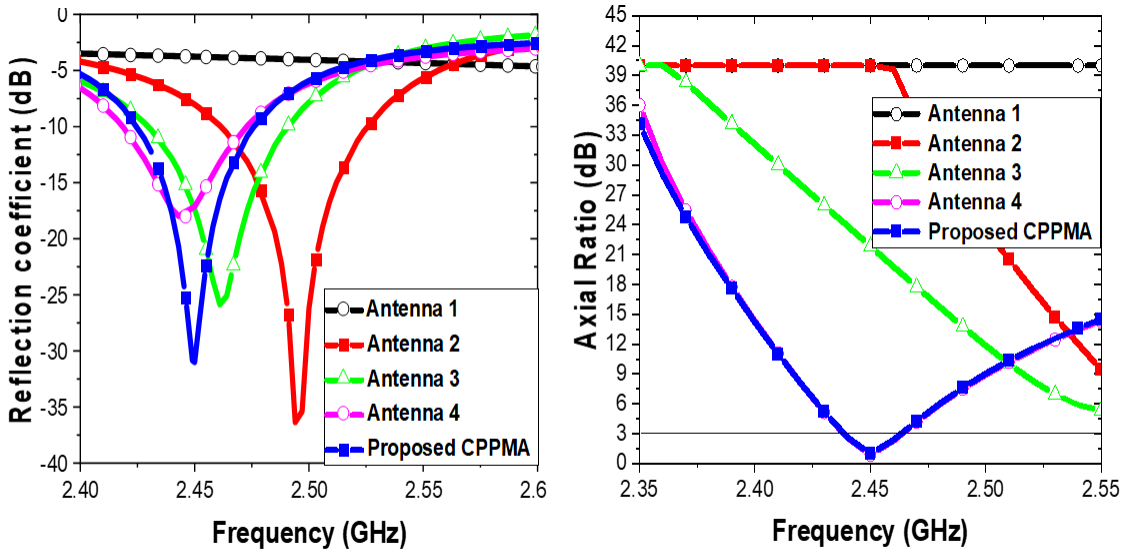

(a) (b)

Fig. 3. (a) Reflection coefficient and (b) AR of the proposed CPPMA compared with the initial reference antennas.

A 3.01 dBi maximum directivity is achieved while a radiation efficiency of 92.49 % is attained at 2.45 GHz.

Figure 6 shows the fabricated prototype of the proposed CPPMA printed on FR4-Epoxy of size 34 × 28 × 1.5 mm^3. The prototype was fabricated using the PCB prototyping machine LPKF Proto Mat E44. Figure 7 presents the reflection coefficient setup measurement using the R&S®ZNB Vector Network Analyzer. Figure 8 shows that the simulated and measured reflection coefficients of the CPPMA are in good agreement. The measured impedance bandwidth ranges between 2.32 GHz and 2.515 GHz while the simulated one varies between 2.425 GHz and 2.475 GHz.

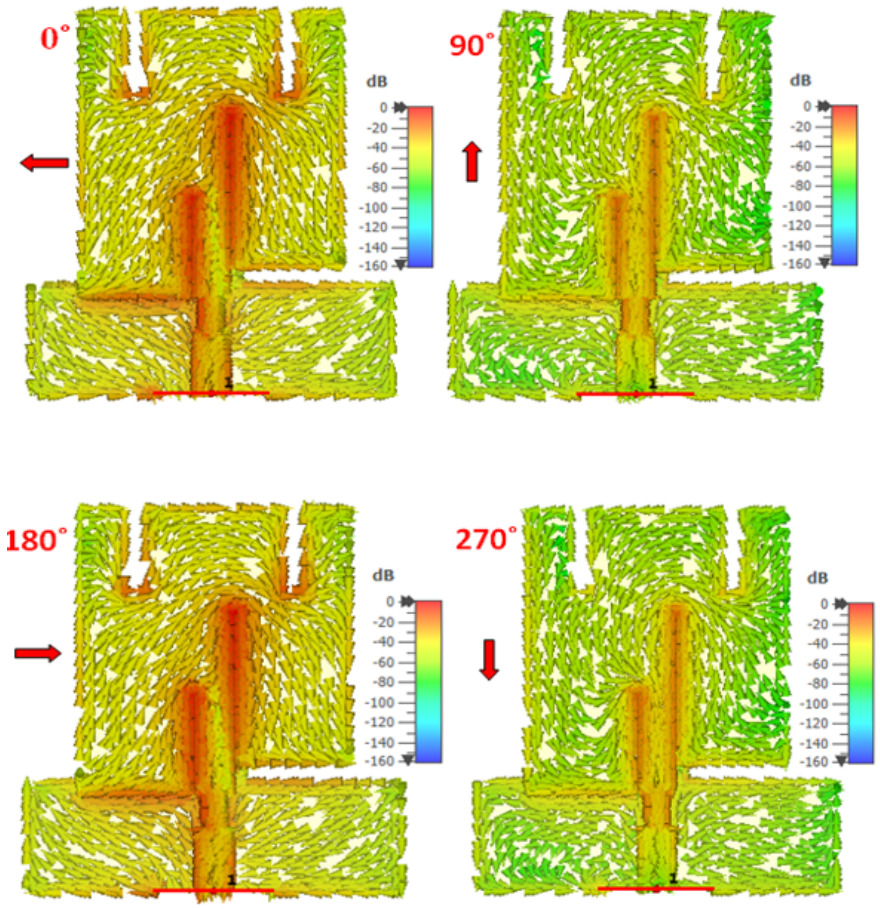

Fig. 4. Surface current distribution on the proposed CPPMA at 2.45 GHz for four different phases: 0°, 90°, 180° and 270°.

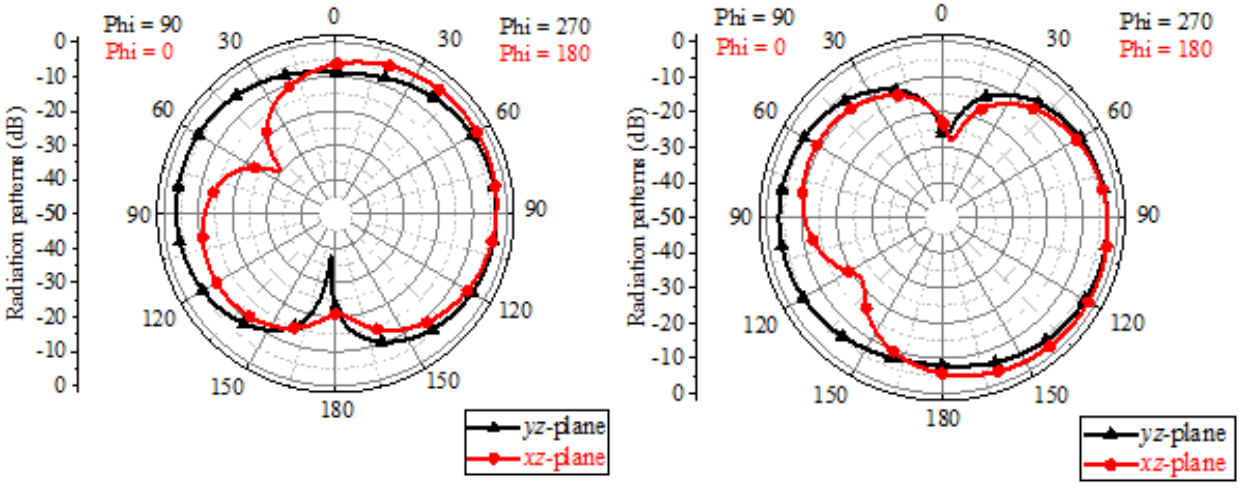

Fig. 5. Radiation patterns of the proposed CPPMA at 2.45 GHz: (a) LHCP and (b) RHCP.

(a) (b)

Fig. 6. Fabricated prototype of the proposed CPPMA: (a) front view and (b) back view.

Fig. 7. Reflection coefficient setup measurement of the proposed CPPMA.

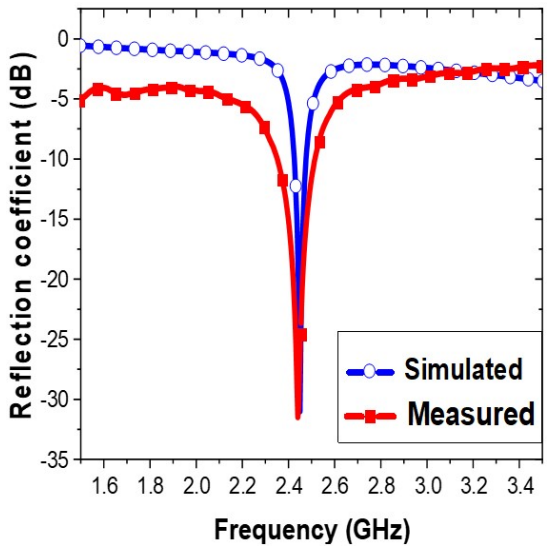

Fig. 8. Simulated and measured reflection coefficient of the proposed CPPMA.

B. Human body phantom models

Various breast, head and arm phantoms have been proposed in the literature. Because various tissues have different electrical properties and absorb different quantities of microwaves, changes in the frequency spectrum have a large influence on the dielectric characteristics of biological tissues [20, 21].

The dielectric properties are reconstructed in quantitative microwave imaging based on the difference in the complex permittivity. Due to the complexity of the structure and composition of biological tissues, Gabriel, et al. [22, 23] used the 4-Cole-Cole model which exhibits a parametric description of four types of dispersion in biological tissue. This model describes the frequency-dependent permittivity and conductivity of several biological tissues in the frequency range from Hz to GHz, which is defined as:

$$\varepsilon(\omega) = \varepsilon'(\omega) + j\varepsilon''(\omega) = \sum_{n=1}^{4} \varepsilon_\infty + \frac{\Delta\,\varepsilon_n}{1+(j\omega\tau_n)^{1-\alpha_n}} + \frac{\sigma_i}{j\omega\varepsilon_0}, \quad (1)$$

where the ability to absorb microwave energy is indicated by the loss factor, whereas the ability to store microwave energy is indicated by the real part. The magnitude of the dispersion is described as $\Delta\,\varepsilon_n = \varepsilon_s - \varepsilon_\infty$, ε_∞ is the permittivity at high frequency, ε_s is the static permittivity, ω is the angular frequency (rad/s), τ is the relaxation time constant (s), σ_i is the static ionic conductivity (S/m), α is a distribution parameter and ε_0 is the permittivity of free space.

The basic principle of the use of microwaves in breast imaging for detecting malignant cells is based on the significant divergence between the dielectric properties of pathological tissues and healthy tissues. In the

breast cancer detection, a mono-static radar imaging system uses one antenna that acts as a transceiver to detect and locate the tumor in the breast with an easier and clearer manner. The antenna transmits microwave pulses toward the breast to scan several locations inside the breast phantom.

The antenna then receives signals from the breast in terms of reflected or scattered signals. It is used to highlight that the changes in the back-scattered signal divulge disparities in the electrical properties of tissues. Thus, the back-scattered signal can be used to find out tumor cells in the breast, which exhibit higher dielectric constants than normal breast tissues [24, 25].

B.1. Human breast phantom model

A hemispherical shaped breast model has been simulated in the present paper. It is composed of 3 layers i.e. skin, fat and fibro-glandular as depicted in Fig. 9. The properties of human breast phantom model [22, 26] and of the tumor model [27, 28] are given in the Table 2.

Table 2: Parameters of the 3-layer human breast phantom model and tumor model at 2.45 GHz

Tissues	ε (F/m)	σ (S/m)	ρ (kg/ m^3)	R (mm)
Skin	38.0067	1.46407	1100	50
Fat	5.14667	0.137039	900	48
Fibro-Glandular	20.1	0.5	1040	38
Tumor	55.2566	2.7015	1050	/

ε = permittivity, σ = electrical conductance, ρ = density, R = radius

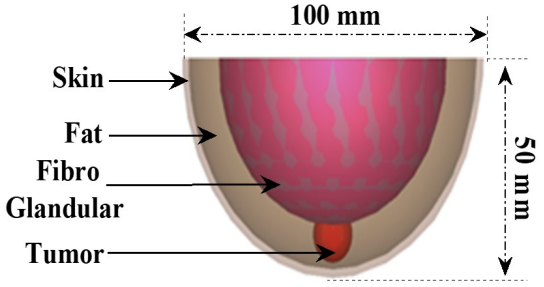

Fig. 9. Hemispherical human breast phantom model.

B.2. Human head phantom model

A spherical-shaped head model was considered in this paper. As depicted in Fig. 10, it is composed of 7 layers, i.e. skin (dry), fat, muscle, skull, dura, cerebrospinal fluid and brain. The properties of the considered human head phantom model and of the stroke model (blood clot) are given in Table 3.

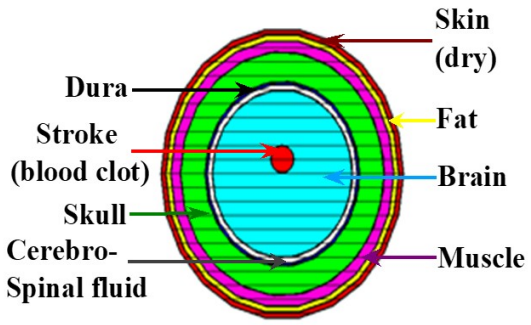

Fig. 10. Spherical human head phantom model.

Table 3: Parameters of the 7-layer human head phantom model and brain stroke model (blood clot) at 2.45 GHz [22, 29]

Tissues	ε (F/m)	σ (S/m)	ρ (kg/ m^3)	R (mm)
Skin	38.0067	1.46407	1100	50
Fat	5.14667	0.137039	900	48
Muscle	53.573540	1.810395	1040.0	46
Skull	14.965101	0.599694	1850.0	42
Dura	42.035004	1.668706	1130	32
Cerebro-spinal Fluid	66.243279	3.457850	1006	31
Brain	42.538925	1.511336	1030.0	29
Stroke (Blood Clot)	58.263756	2.544997	/	/

B.3. Human arm phantom model

A portion of a human arm phantom model has been designed. It is composed of 4 layers, i.e. skin, fat, muscle and bone, as depicted in Fig. 11. The properties of

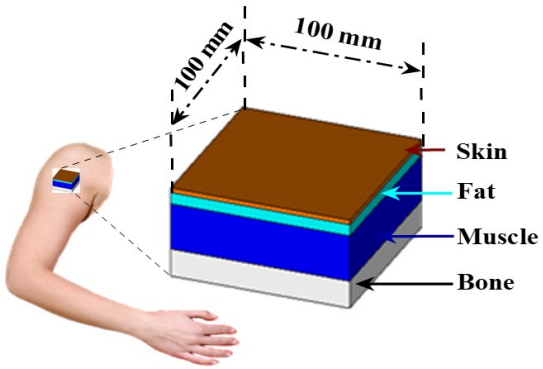

Fig. 11. Portion of a human arm phantom model.

the considered human arm phantom model are given in Table 4 [30].

Table 4: Parameters of the 4-layer human arm phantom model at 2.45 GHz [30]

Tissues	ε (F/m)	σ (S/m)	ρ (kg/m^3)	T (mm)
Skin	37.95	1.49	1001	2
Fat	5.27	0.11	900	5
Muscle	52.67	1.77	1006	20
Bone	18.49	0.82	1008	13

T = thickness

III. SIMULATION AND RESULTS

A. Breast cancer detection

The effect of radiation on the human breast model is examined in this section. First, the proposed CPPMA was positioned at a safe distance of 10 mm from a healthy human breast phantom model as depicted in Fig. 12 (a). Then, a spherical tumor of radius 2.5 mm was inserted at four different positions inside the healthy human breast phantom as depicted in Fig. 12 (b). The reflection coefficient of the designed CPPMA with the human breast model having a tumor (R = 2.5 mm) at four different positions (0, 0, 15), (20, 15, 30), (0, 0, 40), (30, −30, 50) and without the tumor, is shown in Fig. 13. It is clear that the shifting level of the resonant frequency is inversely proportional to the distance between the CPPMA and the tumor.

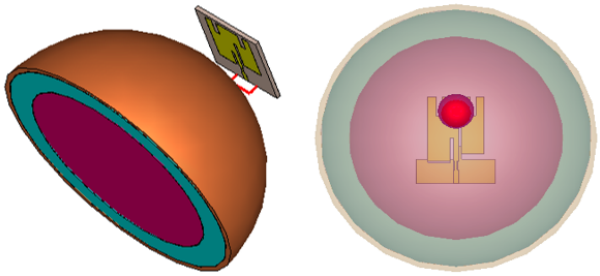

(a) (b)

Fig. 12. CPPMA placed at a distance of 10 mm from the human breast phantom model: (a) without tumor and (b) with tumor.

Then, three different sizes (R = 4 mm, 7 mm and 9 mm) of tumors were placed at a fixed position inside the healthy human breast phantom as depicted in Fig. 12 (b). The reflection coefficient of the set CPPMA and human breast model with and without a tumor is presented in Fig. 14. It reveals that the shift in the resonance

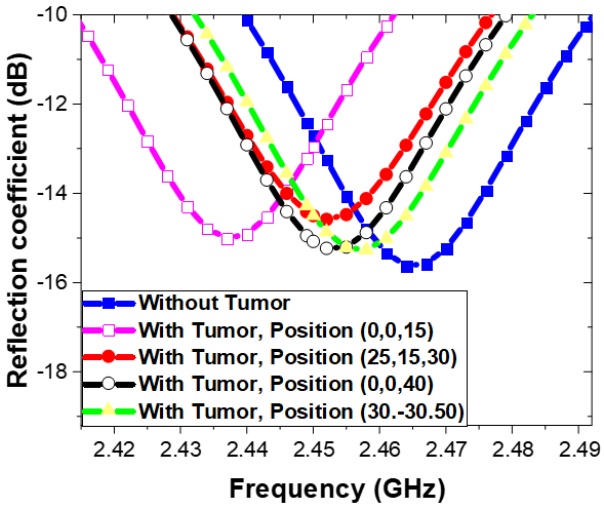

Fig. 13. Simulated reflection coefficient for human breast phantom model in the presence of a tumor of radius = 2.5 mm at 4 different positions.

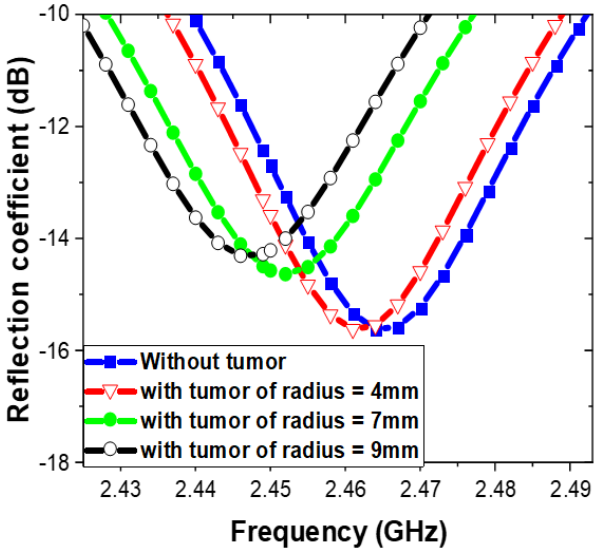

Fig. 14. Simulated reflection coefficient for detecting three different sizes of breast tumor at the same location.

frequency and in the adaptation level is more noticeable for large tumor sizes. Thus, as the tumor size increases, its detection becomes easier.

B. Brain stroke detection

In this section, the effect of radiation on the human head model is discussed. First, the designed CPPMA was positioned at a safe distance of 5 mm from the healthy human head phantom model as depicted in Fig. 15 (a). Then, a brain stroke (blood clot) of two different radiuses 5 and 13 mm, with the dielectric properties depicted in Table 3, was placed inside the healthy brain as depicted

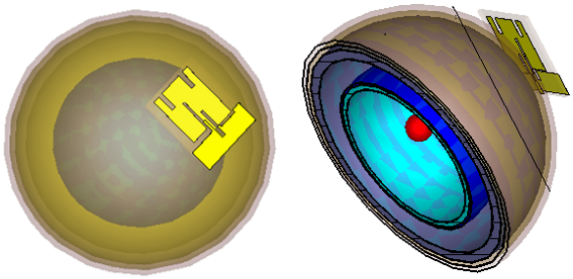

(a) (b)

Fig. 15. CPPMA positioned at a distance of 5 mm from the human head phantom model: (a) without brain stroke, and (b) with brain stroke (blood clot).

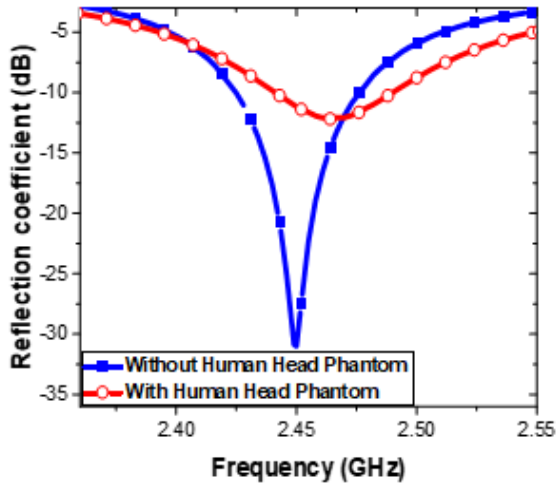

(a)

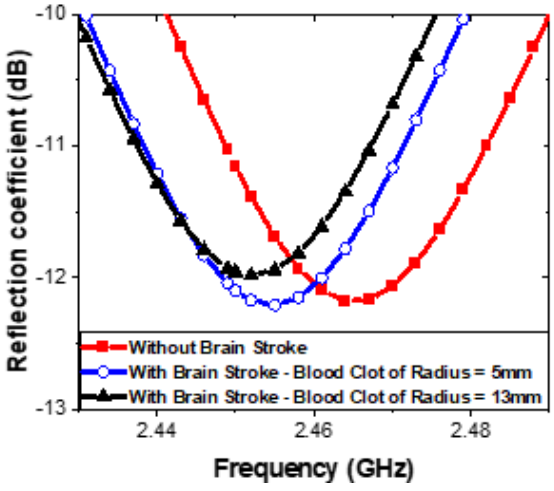

(b)

Fig. 16. (a) Simulated reflection coefficient with and without human head phantom model, (b) simulated reflection coefficient for detecting two different sizes of stroke (blood clot).

in Fig. 15 (b). The reflection coefficient of the set CPPMA and human head model with and without stroke (blood clot) is shown in Fig. 16. A shift in the resonance frequency of the CPPMA in the cases of normal and brain stroke is clear. The reflected wave increases with the increase in the size of the blood clots which agree with expectation.

Figures 17–19 show the simulated E-field, H-field and current density of the set CPPMA and human head model with and without stroke at 2.45 GHz. Table 5 indicates that the current density, E-field and H-field values decrease in the presence of brain stroke which predict its existence in the human head.

Table 5: Comparison of the simulated results with and without brain stroke model at 2.45 GHz

	Without Brain Stroke	**With Brain Stroke R = 5 mm**	**With Brain Stroke R = 13 mm**
Resonance Frequency (GHz)	2.464	2.455	2.452
Reflection Coefficient (dB)	−12.142075	−12.207286	−11.97995
Current Density A/m^2	683.562	639.836	636.324
E Field V/m	71078.5	59542.3	62530
H Field A/m	770.724	545.151	505.475

The linearly-polarized antenna shown in Fig. 2 (b) has been simulated without and with a brain stroke model (R = 5 mm and 13 mm) to show the advantages of the circular polarization for the detection of the brain stroke. Slight adjustments have been introduced in the dimensions of the antenna to shift the resonant frequency to 2.45 GHz.

The reflection coefficient of the simulated linearly polarized printed monopole antenna (LPPMA) is presented in Fig. 20. The reflection coefficient of the set LPPMA and human head model with and without the stroke model is shown in Fig. 22.

It reveals that there is no shift in the resonance frequency compared to the results obtained with the proposed CPPMA (Fig. 16 (b)). Table 6 indicates that the CPPMA is more effective than the LPPMA in detecting brain stroke because the circularly polarized waves penetrate the body more deeply.

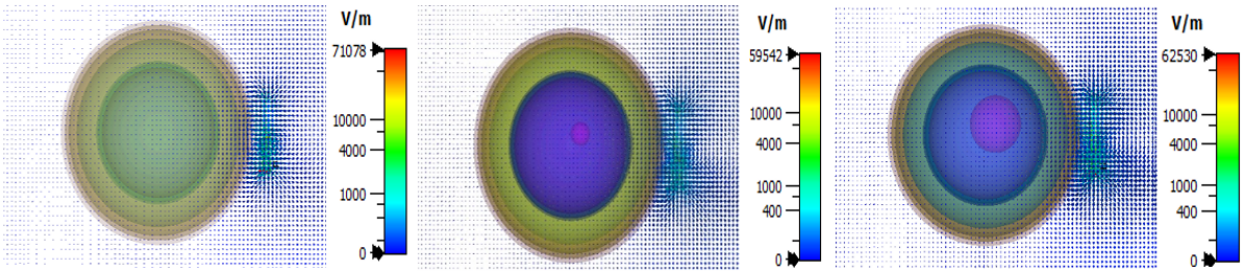

(a) (b) (c)

Fig. 17. Electric field: (a) without brain stroke, (b) with stroke R = 5mm, and (c) with stroke R = 13mm.

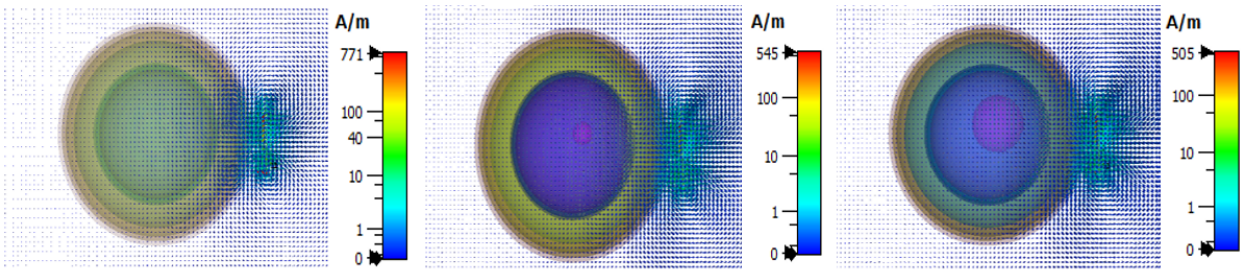

(a) (b) (c)

Fig. 18. Magnetic field: (a) without brain stroke, (b) with stroke R = 5mm, and (c) with stroke R = 13mm.

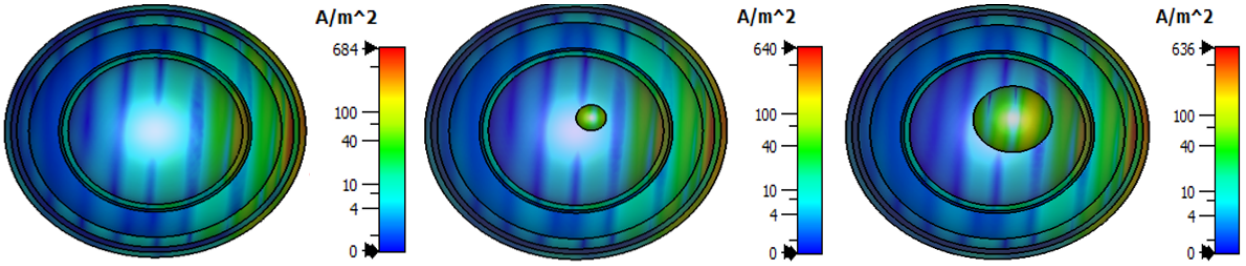

(a) (b) (c)

Fig. 19. Current density: (a) without brain stroke, (b) with stroke R = 5mm, and (c) with stroke R = 13mm.

Table 6: Comparison of the simulated results of the two antennas CPPMA and LPPMA with and without brain stroke model

		Without Brain Stroke	**With Brain Stroke R = 5 mm**	**With Brain Stroke R = 13 mm**
CPPMA	Resonance Frequency (GHz)	2.464	2.455	2.452
	Reflection Coefficient (dB)	−12.14207	−12.207286	−11.97995
LPPMA	Resonance Frequency (GHz)	2.467	2.467	2.467
	Reflection Coefficient (dB)	−13.50134	−13.485089	−13.45988

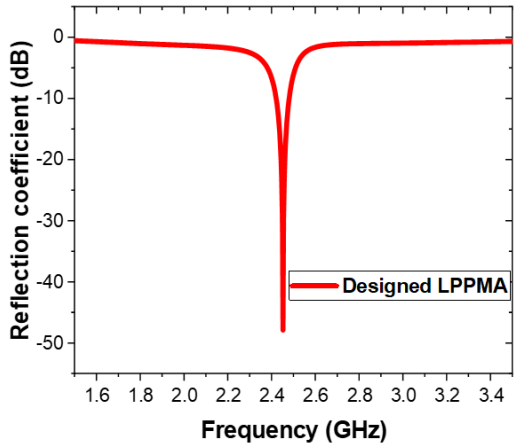

Fig. 20. Reflection coefficient of the designed LPPMA.

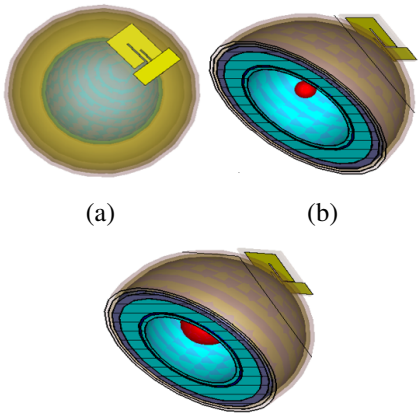

(a) (b)

(c)

Fig. 21. LPPMA placed at a distance of 5 mm from the human head phantom model: (a) without brain stroke, (b) with brain stroke R = 5 mm, and (c) with brain stroke R = 13 mm.

IV. WEARABLE APPLICATION

In this section, the CPPMA performance has been simulated on a human arm phantom model and on a human arm to check its usefulness for health monitoring and wearable application. First, the designed CPPMA was positioned at a safe distance of 10 mm from a human arm phantom model as depicted in Fig. 23 (a). Figure 23 (b) indicates that the resonant frequency of the CPPMA positioned on a human arm phantom model has a small shifting compared to the antenna without a human arm phantom due to the high dielectric proprieties of body tissues. Nonetheless, the designed CPPMA in the presence of a human arm phantom has an impedance bandwidth extending from 2.438 GHz to 2.489 GHz with a reflection coefficient level of −13.28 dB which covers the desired ISM band.

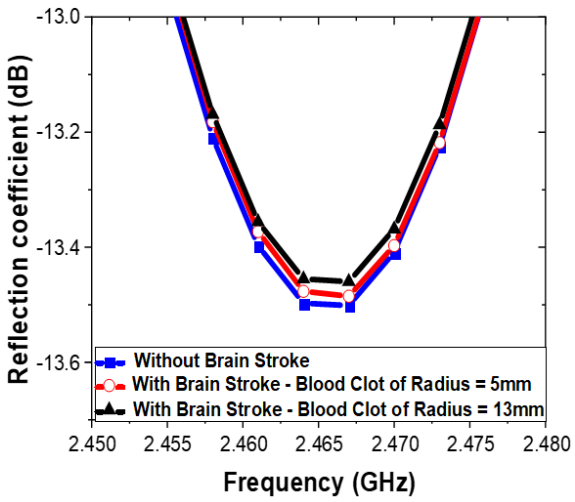

Fig. 22. Simulated reflection coefficient of the LPPMA for detecting two different sizes of brain stroke model.

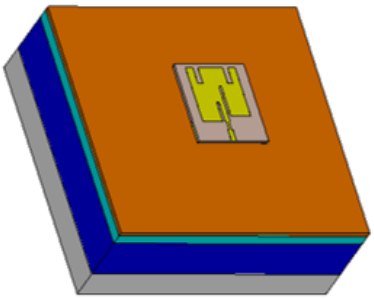

(a)

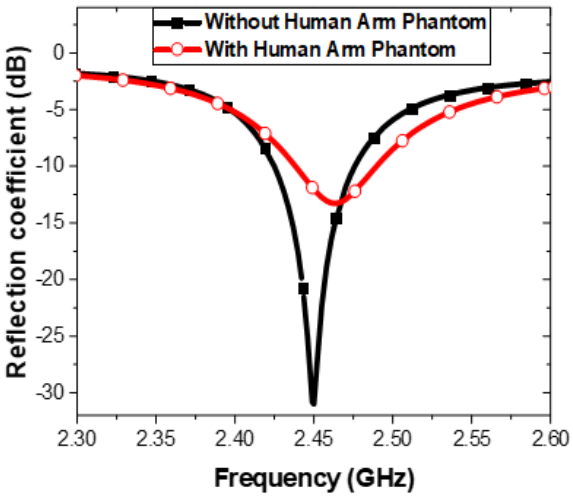

(b)

Fig. 23. (a) CPPMA placed at a distance of 10 mm from the portion of a human arm phantom model and (b) simulated reflection coefficient with and without human arm phantom.

The usefulness of the proposed CPPMA for wearable health-monitoring applications was checked experimentally by placing the fabricated prototype on a human arm as shown in Fig. 24. The simulated and measured reflection coefficient results of the proposed CPPMA placed on a human arm are compared in Fig. 25.

The volume of the human arm, the gap between the CPPMA and the human arm, and SMA losses were the causes of the mismatch between the on-arm simulated and measured values. We conclude from the results that the proposed CPPMA is suitable for wearable health-monitoring applications.

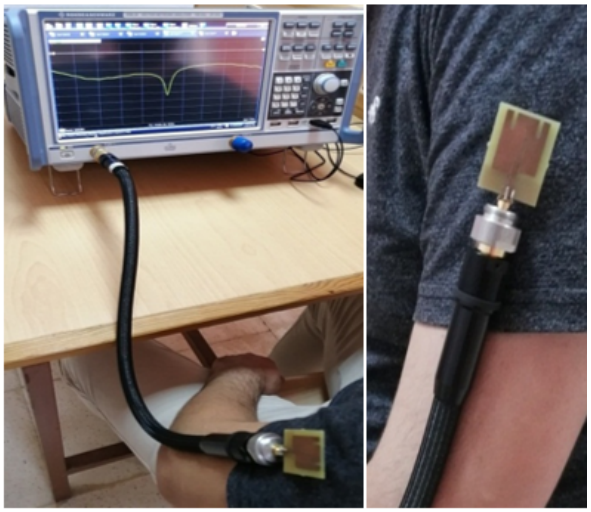

Fig. 24. Reflection coefficient measurement of the fabricated prototype on a human arm.

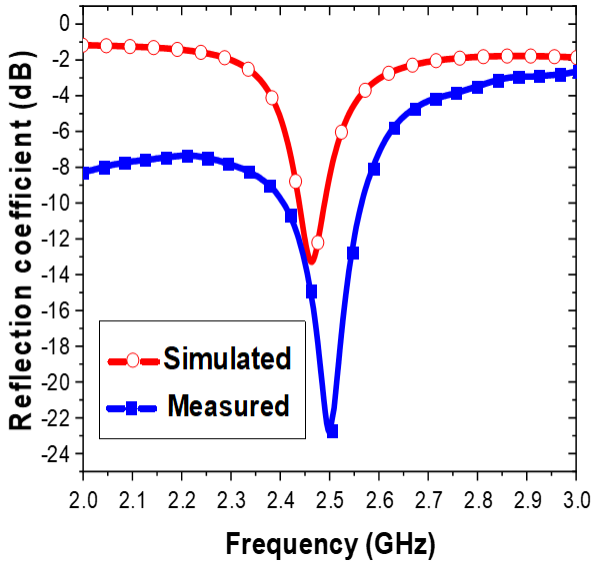

Fig. 25. Reflection coefficient of the proposed CPPMA on a human arm.

V. SPECIFIC ABSORPTION RATE (SAR) CALCULATIONS

SAR describes how much power is absorbed per kilogram of human body tissue. Hence, its unit is Watts per Kilogram (W/Kg). Typically the SAR is averaged across a small volume (1 g or 10 g) of tissue. Its value is calculated using the following equation [31]:

$$SAR = \frac{\sigma}{\rho}|E|^2 = \frac{J^2}{\rho\sigma}, \tag{2}$$

where, E is the electric field intensity in V/m, J is the current density in A/m, σ is the electric conductivity of the tissue in S/m, and ρ is mass density of the tissue in Kg/m^3.

In this section, the SAR parameter of the proposed CPPMA was analyzed on the breast, head and arm of the human body phantom.

The SAR values refer to power averaged over 10 g of tissue. In order to satisfy the most restrictive SAR regulation (i.e. $SAR_{10g} < 2$ W/kg), the input powers must be limited according to Table 7.

Table 7: Input power limits that give acceptable SAR_{10g} values at 2.45 GHz

	Distance (mm)	Input Power (mW)	SAR_{10g} (W/Kg)
Breast	10	110	1.84
Head	5	68	1.9
Arm	10	170	1.92

The simulated SAR_{10g} on the breast, head and portion of a human arm is shown in Fig. 26.

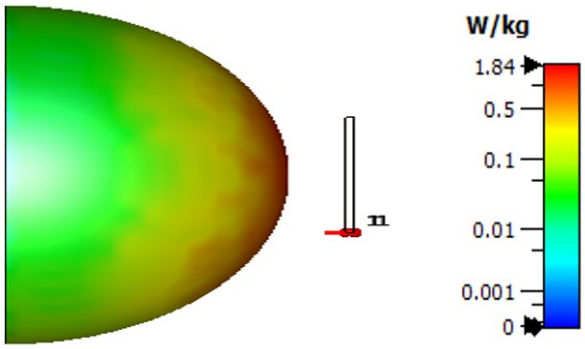

(a)

Fig. 26. *Continued.*

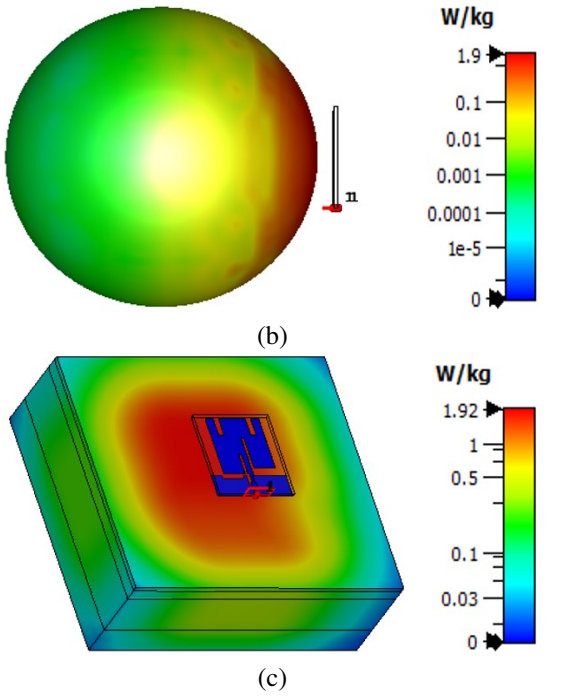

Fig. 26. Simulated specific absorption rate (SAR_{10g}) at 2.45 GHz: (a) breast, (b) head, and (c) portion of a human arm phantom model.

VI. CONCLUSIONS

This paper presented a mono-static narrow band CPPMA for medical microwave imaging and health monitoring applications. A prototype of the designed CPPMA of size 34 × 28 × 1.5 mm^3 has been fabricated and printed on the low-cost FR-4 substrate. The measured results indicate that the fabricated prototype operates in a narrow bandwidth of 195 MHz (2.32 - 2.515 GHz). Moreover, the designed CPPMA exhibits a circular polarization in the range of 2.4386 - 2.4633 GHz. The capability of the detection of breast tumor and brain stroke for the proposed CPPMA was validated using different phantom models.

Furthermore, the practicality of the proposed CPPMA for wearable health-monitoring applications was confirmed experimentally. The overall obtained results confirm the effectiveness and usefulness of the proposed CPPMA for several biomedical applications.

ACKNOWLEDGMENT

This work is supported by the Ministry of Higher Education and Scientific Research of Algeria, as part of a research project (PRFU N^o, A25N01UN240120220002).

Table 8: Comparison of the proposed CPPMA with several recently reported antennas

Ref.	Application	Technique Used for Pathological Tissue Detection	Substrate and Dimensions (mm^3)	Circular Polar	Frequency Band (GHz)	SAR Evaluation
[32]	Body-centric communications	-	RO4003 42 × 30 × 0.813	No	2.4 - 12	Not reported
[33]	Breast tumor detection	Scattering imaging	Air-gap 40 × 25 × 10.5	No	1.67 - 1.74	Not reported
[34]	Breast tumor detection	Resonance frequency shift	RO4003C 40 × 40 × 1.54	No	0.49 - 0.56	Not reported
[35]	Wireless body area network	-	RT-Duroid 5880 34.4 × 34.4 × 4	Yes	5.27 - 6.37	SAR evaluated on human body
[36]	Head imaging	Scattering parameters and near field directivity	RO4350B 50 × 44 × 1.524	No	1.70 - 3.71	SAR evaluated on head
[37]	Wireless body area network	-	Denim 50 × 44 × 0.7	No	2.27 - 3.42	SAR evaluated on human body arm
This work	**Tumor detection, brain stroke detection and remote health monitoring**	**Resonance frequency shift, current density, E-Field and H-Field distribution**	**FR-4 34 × 28 × 1.5**	**Yes**	**2.425 - 2.475**	**SAR evaluated on breast, head and human body arm**

REFERENCES

[1] K. Lalitha and J. Manjula, "Non-invasive microwave head imaging to detect tumors and to estimate their size and location," *Phys. Med*, vol. 13, pp. 100047, 2022.

[2] M. A. Aldhaeebi, K. Alzoubi, T. S. Almoneef, S. M. Bamatraf, H. Attia, and O. M. Ramahi, "Review of microwaves techniques for breast cancer detection," *Sensors*, vol. 20, no. 8, pp. 2390, 2020.

[3] G. Kaur and A. Kaur, "Monostatic radar-based microwave imaging of breast tumor detection using a compact cubical dielectric resonator antenna," *Microw. Opt. Technol. Lett.*, vol. 63, no. 1, pp. 196-204, 2021.

[4] W. He, Y. He, S. W. Wong, and C. H. Liao, "A wideband circularly polarized S-shaped slot antenna," *Int. J. RF Microw. Comput.-Aided Eng.*, vol. 31, no. 5, pp. e22612, 2021.

[5] N. Sharma, A. Kumar, A. De, and R. K. Jain, "Design of compact hexagonal shaped multiband antenna for wearable and tumor detection applications," *Prog. Electromagn. Res. M*, vol. 105, pp. 205-217, 2021.

[6] R. Alageea and A. Assalem, "Brain cancer detection using U-shaped slot vivaldi antenna and confocal radar based microwave imaging algorithm," *Am. Sci. Res. J. Eng. Technol. Sci*, vol. 66, no. 1, pp. 1-13, 2020.

[7] M. Samsuzzaman, K. A. Fakeeh, M. S. Talukder, M. M. Hasan, M. H. Rahman, M. M. Alam, M. S. Shaik, and M. T. Islam, "A double hollow rectangular-shaped patch and with the slotted ground plane monopole wideband antenna for microwave head imaging applications," *Int. J. Commun. Syst*., vol. 34, no. 16, pp. e4958, 2021.

[8] N. Niranjankumar, B. S. Srikanth, S. B. Gurung, S. Manu, G. N. S. Gowthami, T. Ali, and S. Pathan, "A slotted UWB monopole antenna with truncated ground plane for breast cancer detection," *Alex. Eng. J.*, vol. 59, no. 5, pp. 3767-3780, 2020.

[9] A. B. Dey, S. S. Pattanayak, D. Mitra, and W. Arif, "Investigation and design of enhanced decoupled UWB MIMO antenna for wearable applications," *Microw. Opt. Technol. Lett.*, vol. 63, no. 3, pp. 845-861, Mar. 2021.

[10] U. R. Khan, J. A. Sheikh, S. Bashir, and S. Ahmed, "Metamaterial inspired wideband on-body antenna design for bio-medical applications," *Mater. Today: Proc.*, vol. 80, no. 3, pp. 1772-1776, 2023.

[11] H. Singh, K. Srivastava, S. Kumar, and B. K. Kanaujia, "A planar dual-band antenna for ISM/wearable applications," *Wirel. Pers. Commun.,* vol. 118, no. 1, pp. 631-646, 2021.

[12] Y. K. Ho, T. E. M. Foong, H. Takefumi, L. K. Chun, and H. Kazuhiro, "A multi-band planar antenna for biomedical applications," *Frequenz*, vol. 75, no. 5-6, pp. 221-228, 2021.

[13] S. Roy and U. Chakraborty, "Metamaterial based dual wideband wearable antenna for wireless applications," *Wirel. Pers. Commun.*, vol. 106, no. 3, pp. 1117-1133, June 2019.

[14] K. Zhang, P. J. Soh, and S. Yan, "Design of a compact dual-band textile antenna based on metasurface," *IEEE Trans. Biomed. Circuits Syst*., vol. 16, no. 2, pp. 211-221, Apr. 2022.

[15] X. Lin, Y. Chen, Z. Gong, B. C. Seet, L. Huang, and Y. Lu, "Ultrawide band textile antenna for wearable microwave medical imaging applications," *IEEE Trans. Antennas Propag*., vol. 68, no. 6, pp. 4238-4249, June 2020.

[16] K. Zhang, G. A. E. Vandenbosch, and S. Yan, "A novel design approach for compact wearable antennas based on metasurfaces," *IEEE Trans. Biomed. Circuits Syst*., vol. 14, no. 4, pp. 918-927, Aug. 2020.

[17] O. Fiser, V. Hruby, J. Vrba, T. Drizdal, J. Tesarik, and D. Vrba, "UWB bowtie antenna for medical microwave imaging applications," *IEEE Trans. Antennas Propag*., vol. 70, no. 7, pp. 5357-5372, July 2022.

[18] A. Chaabane and M. Guerroui, "Circularly polarized ultra wideband antenna with question mark-shaped patch for ground penetrating radar applications," *J. Appl. Res. Technol*., vol. 20, no. 3, pp. 274-283, June 2022.

[19] A. Chaabane, M. Guerroui, and D. Aissaoui, "Circularly polarized quasi-rectangular patch UWB antenna for GPR applications," *Serb. J. Electr. Eng*., vol. 19, no. 3, pp. 261-271, Oct. 2022.

[20] S. Gabriel, R. W. Lau, and C. Gabriel, "The dielectric properties of biological tissues: II. Measurement in the frequency range 10 GHz to 20 GHz," *Phys. Med. Biol*., vol. 41, no. 11, pp. 2251- 2269, 1996.

[21] L. Farrugia, P. S. Wismayer, L. Z. Mangion, and C. V. Sammut, "Accurate in-vivo dielectric properties of liver from 500 MHz to 40 GHz and their correlation to ex-vivo measurements," *Electromagn. Biol. Med*., vol. 35, no. 4, pp. 365-373, 2016.

[22] C. Gabriel, "Compilation of the dielectric properties of body tissues at RF and microwave frequencies," *U.S. Air Force Report* AFOSR-

TR-96. Available at: https://www.fcc.gov/general/body-tissue-dielectric-parameters, 1996.

[23] N. De Geeter, G. Crevecoeur, L. Dupré, W. V. Hecke, and A. Leemans, "A DTI-based model for TMS using the independent impedance method with frequency-dependent tissue parameters," *Phys. Med. Biol.*, vol. 57, no. 8, pp. 2169-2188, 2012.

[24] I. R. Sheeba and T. Jayanthy, "Design and analysis of a flexible softwear antenna for tumor detection in skin and breast model," *Wireless Pers. Commun.*, vol. 107, no. 2, pp. 887-905, 2019.

[25] R. Singh, N. Narang, D. Singh, and M. Gupta, "Compact wideband microstrip patch antenna design for breast cancer detection," *Def. Sci. J.*, vol. 71, no. 3, pp. 352-358, May 2021.

[26] Z. Katbay, S. Sadek, R. Lababidi, A. Perennec, and M. le Roy, "Miniature antenna for breast tumor detection," *IEEE NEWCAS 13th International New Circuits and Systems Conference*, Grenoble, France, pp. 1-4, 2015.

[27] R. Ortega-Palacios, L. Leija, A. Vera, and M. F. J. Cepeda, "Measurement of breast-tumor phantom dielectric properties for microwave breast cancer treatment evaluation," *IEEE 7th International Conference on Electrical Engineering Computing Science and Automatic Control.*, Tuxtla Gutierrez, Mexico, pp. 216-219, 2010.

[28] M. Palandoken, C. Murat, A. Kaya, and B. Zhang, "A novel 3-D printed microwave probe for ISM band ablation systems of breast cancer treatment applications," *IEEE Trans. Microw. Theory Tech.*, vol. 70, no. 3, pp. 1943-1953, Mar. 2022.

[29] M. A. Rahman, M. F. Hossain, M. A. Riheen, and P. K. Sekhar, "Early brain stroke detection using flexible monopole antenna," *Prog. Electromagn. Res. C*, vol. 99, pp. 99-110, 2020.

[30] S. Kiani, P. Rezaei, and M. Fakhr, "A CPW-fed wearable antenna at ISM band for biomedical and WBAN applications," *Wirel. Netw.*, vol. 27, no. 1, pp. 735-745, 2021.

[31] M. K. Hosain, A. Z. Kouzani, S. J. Tye, O. A. Abulseoud, A. Amiet, A. Galehdar, and M. Berk, "Development of a compact rectenna for wireless powering of a head-mountable deep brain stimulation device," *IEEE J. Transl. Eng. Health Med.,* vol. 2, pp. 1-13, 2014.

[32] A. Darvazehban and T. Rezaee, "Ultra-wideband microstrip antenna for body centric communications," *Applied Computational Electromagnetics Society (ACES) Journal*, vol. 33, no. 3, pp. 355-358, Mar. 2018.

[33] M. A. Ullah, T. Alam, M. S. Alam, S. Kibria, and M. T. Islam, "A unidirectional 3D antenna for biomedical microwave imaging based detection of abnormality in human body," *Microsyst. Technol.*, vol. 24, no. 12, pp. 4991-4996, 2018.

[34] M. A. Aldhaeebi, T. S. Almonee, H. Attia, and O. M. Ramahi, "Electrically small magnetic probe with PCA for near-field microwave breast tumors detection," *Prog. Electromagn. Res. M*, vol. 84, pp. 177-186, 2019.

[35] Y. B. Chaouche, M. Nedil, I. B. Mabrouk, and O. M. Ramahi, "A wearable circularly polarized antenna backed by AMC reflector for WBAN communications," *IEEE Access*, vol. 10, pp. 12838-12851, 2022.

[36] A. Hossain, M. T. Islam, M. E. Chowdhury, and M. Samsuzzaman, "A grounded coplanar waveguide-based slotted inverted delta-shaped wideband antenna for microwave head imaging," *IEEE Access*, vol. 8, pp. 185698-185724, 2020.

[37] D. Gopi, P. V. Kokilagadda, S. Gupta, and V. R. K. R. Dodda, "Asymmetric coplanar strip-fed textile-based wearable antenna for MBAN and ISM band applications," *Int. J. Numer. Model: Electron. Netw. Devices Fields*, vol. 34, no. 6, pp. e2920, 2021.

Bilal Guetaf is currently a Ph.D. Student at the University 8 Mai 1945 Guelma, Algeria. He is a member of the Telecommunications Laboratory, University 8 Mai 1945 Guelma. His main research interests include: antennas for medical microwave imaging, wearable antennas, implantable antennas, and biomedical engineering.

Abdelhalim Chaabane received a Ph.D. degree and completed his habilitation in electronics in 2017 and 2020, respectively. He is currently an associate professor and the Director of the Telecommunications Laboratory at the University 8 Mai 1945 Guelma, Algeria. His current research areas of interest include: fractal antennas, MIMO antenna systems, reconfigurable antennas, millimeter-wave high-gain and wide-band antennas, UWB applications and radar, and biomedical engineering.

Abderrezak Khalfallaoui received a Ph.D. degree in Electronics from the University of Littoral Côte d'Opale, France, in 2010 at the Laboratory of Materials and Components for Electronics (LEMCEL). In 2011, he joined the Telecommunications Laboratory at the University 8 Mai 1945 Guelma, Algeria where he is an Assistant Professor. His research interests are design and processing of radio-frequency integrated circuits, tunable ferroelectric devices, and their applications in microwaves. Since 2020, his research has been on antennas, multiband antennas, and ground-penetrating radar antennas.

Hussein Attia received a Ph.D. in Electrical and Computer Engineering from the University of Waterloo, Ontario, Canada, in 2011. He worked as a Research Engineer with the Coding and Signal Transmission Laboratory at the University of Waterloo from March 2011 to July 2013. He was granted a Postdoctoral Fellowship at Concordia University, Montreal, Canada, from August 2014 to July 2015. He was also a Visiting Scholar at the University of Quebec (INRS), from August 2015 to December 2015 and from June 2017 to August 2017. He is currently an Associate Professor and the Director of the Applied Electromagnetics Laboratory at King Fahd University of Petroleum and Minerals (KFUPM). He is currently an Associate Editor for IEEE Antennas and Wireless Propagation Letters and IEEE ACCESS. He has published about 100 journaln and conference papers. His research interests include biomedical engineering, microwave sensors, millimeter-wave antennas, analytical techniques for electromagnetic modeling, and metamaterials. Dr. Attia has received several awards, including a full Ph.D. scholarship from the Ministry of Higher Education, Egypt (2007-2011), the University of Waterloo Graduate Scholarship for excellence in research and coursework in 2009, and a certificate in University Teaching from the University of Waterloo in 2010. He was a finalist in the Best Paper Competition of the 2011 IEEE AP-S International Symposium on Antennas and Propagation. In 1999 he was ranked first among all B.Sc. electronics and communication engineering students at Zagazig University, Egypt.